Acta Cryst. (1997). D**53**, 588–595

X-ray Topography of Tetragonal Lysozyme Grown by the Temperature-Controlled Technique

V. STOJANOFF,[a]† D. P. SIDDONS,[a] LISA A. MONACO,[b] PETER VEKILOV[c] AND FRANZ ROSENBERGER[c]

[a]*NSLS, PO Box 5000, Brookhaven National Laboratory, Upton, NY 11973, USA, and* [b]*Center for Microgravity and Materials Research, University of Alabama in Huntsville. Huntsville, AL 35899, USA. E-mail: siddons@bnl.gov*

(*Received 1 April 1996; accepted 15 April 1997*)

Abstract

Growth-induced defects in lysozyme crystals were observed by white-beam and monochromatic X-ray topography at the National Synchrotron Light Source (NSLS) at the Brookhaven National Laboratory (BNL). The topographic methods were non-destructive to the extent that traditional diffraction data collection could be performed to high resolution after topography. It was found that changes in growth parameters, defect concentration as detected by X-ray topography, and the diffraction quality obtainable from the crystals were all strongly correlated. In addition, crystals with fewer defects showed lower mosaicity and higher diffraction resolution as expected.

1. Introduction

X-ray topography is a non-destructive technique for imaging microscopic structural defects in nearly perfect crystals. It has been applied to a large variety of inorganic and organic materials and undoubtedly has played a major role in the search of defect-free crystals for the semiconductor industry. A review of the different topographic methods, the dynamical theory and its application to different materials can be found in Tanner (1976). To the authors' knowledge no in-depth X-ray topographic study of protein crystals has been performed to date.

In X-ray topography, usually the whole crystal is immersed in a parallel X-ray beam and the resulting diffraction spots are imaged with high spatial resolution. The crystalline defects cause each diffraction spot to contain microscopic intensity variations which can be used to extract information about the type and volume distribution of the defects. This technique works best when the defect density is low and is complementary to the more usual rocking-curve measurements which work best for crystals with high defect densities. Two different X-ray topographic techniques are usually employed. The white-beam, or Laue geometry, provides rapid imaging, but can result in lower effective resolution, particularly in less perfect samples. It is, however, an ideal tool for screening, since exposures are short and alignment is not critical. Monochromatic beam methods can provide more detailed information about defects but require more careful alignment and longer exposures.

In the last 20 years, substantial efforts have been made to study the crystallization of biological macromolecules. The goal has been to find growth conditions yielding higher quality crystals for molecular structure studies. Yet, even for a simple system, such as hen egg-white lysozyme (HEWL) the effect of the growth environment on growth kinetics and dynamics is still not completely understood. With respect to factors that possibly influence the structural quality, optical interferometric investigations have shown that higher solution purity results in different growth facet morphology (Vekilov, Monaco & Rosenberger, 1995), in higher tangential step velocity, and in improved optical homogeneity of lysozyme crystals (Vekilov & Rosenberger, 1996). Also of interest for the dependence of defect formation on growth conditions is the finding that temperature changes as small as 0.1 K can result in striations (veils) in lysozyme crystals (Monaco & Rosenberger, 1993). The purpose of the present study is to characterize by X-ray diffraction topography the defects that result under certain growth conditions, and to attempt to correlate them to standard diffraction statistics.

2. Samples

Tetragonal hen egg-white lysozyme crystals ($P4_32_12$, $a = b = 79.1$, $c = 37.9$ Å) were grown by the temperature-programming technique (Rosenberger, Howard, Sowers & Nyce, 1993). 15–20 µl of growth solution containing 50 mg ml^{-1} lysozyme and 2.5%(*w*/*v*) NaCl in 50 m*M* acetate/acetic acid buffer, pH = 4.5, as described in the previous reference and in Monaco & Rosenberger (1993), were sealed in square glass capillaries (Wilson Scientific Glass, Inc.), which were appropriate for X-ray exposure. A very small portion of the capillary, about 1 mm of the 5 cm long capillary, was kept in thermal contact with a miniature thermoelectric pump (Peltier) that could be programmed between 281 and 323 K. The whole setup, capillary and thermoelectric pump was kept in a temperature-controlled jacket (±0.1 K). Growth was observed by means of a Wild long focal

† Present address: European Synchrotron Radiation Facility, BP 220, 38043 Grenoble CEDEX, France.

Table 1. *Summary of growth, storage and shipping conditions of the HEWL crystals*

Sample	Lysozyme source	Nucleation	Growth		Storage		Shipping	
		T (K)	T (K)	Duration (d)	T (K)	Duration (d)	T (K)	T at arrival (K)
14	Sigma	291.5	291.5	5	299	28	301	298
25-1	Sigma	287.5	287.5	4	299	35	301	297
25-2	Sigma	287.5	287.5	6	299	35	301	297
26-1	Seikagaku	284	284	3	299	20	301	297
26-3	Seikagaku	294	284	3	299	20	301	297
28-c	Seikagaku	283	287, 288	1, 1	301	32	301	296
28-c	Seikagaku	283	286, 287	1, 1	381	32	381	296
28-c	Seikagaku	283	286, 288, 287	1, 1, 1	381	32	381	296

length microscope. Several parameters such as lysozyme suppliers and nucleation and growth temperatures were changed. Lysozyme from two different suppliers, Sigma Chemical Co. and Seikagaku America Inc. was used. Both batches contained higher molecular weight proteins as impurities, Sigma 5.7%(*w*/*w*) and Seikagaku 1.5%(*w*/*w*) as was shown by Thomas, Vekilov & Rosenberger (1996) and Rosenberger, Muschol, Thomas & Vekilov (1996). The temperature history for the different crystals is listed in Table 1. Nucleation and growth temperatures were optimized for each growth condition by optical interferometry. Several nucleation and growth temperatures were selected and the crystals analysed by optical interferometry. When optical interferometry indicated good crystal growth conditions crystals for X-ray analysis were grown under these conditions. The optimal conditions showed to be different for the two different starting materials. Once crystals reached sizes between 0.5 and 0.7 mm they were stored in an incubator at 299 K until beamtime was available.

In order to minimize dissolution or unwanted secondary crystallization during transportation until exposure to the X-ray beam the capillaries were kept immersed in a bath of partly molten octadecane ($C_{18}H_{38}$). The octadecane was heated and its temperature allowed to equilibrate with the temperature in the incubator. It was then packed into a Styrofoam box around a copper cylinder which was in contact with a glass cylinder in which the capillaries had been carefully mounted for transport. A digital thermometer was kept in the Styrofoam box and in contact with the glass cylinder with the crystal capillaries. The thermometer allowed for the temperature to be monitored between the time the crystals were removed from the incubator to the time they were exposed to the X-rays. The temperature change observed was smaller then 3–4 K. Just before exposure the capillaries were opened and the growth solution drained. The surroundings of the crystal were dried until only a thin liquid meniscus layer kept the crystal attached to the capillary wall. Before the capillary was sealed again a small drop of growth solution was inserted on both ends of the capillary to prevent the crystal drying out. During this procedure special care was taken not to touch the crystal.

3. Methods

White and monochromatic synchrotron radiation from beamline X26C at the National Synchrotron Light Source (NSLS) at BNL were employed in the X-ray topographic studies. The X26C port is 20 m from the bending magnet and the spot size at the sample was reduced by several slit assemblies to 1 mm^2. In both cases a helium-filled volume between the acceptance slit and the sample was used to reduce X-ray scattering by air. The diffraction images were recorded on Kodak INDUSTREX SR5 film, which was always kept normal to the incident-beam direction to simplify indexing.

For the white-beam X-ray topography the sample-to-film distance was of the order of 300 mm with an average exposure time of 30 s. The distance was chosen in order to avoid spot overlaps, however, the geometric resolution was shown to be compromized. The diffraction patterns were scanned with a microdensitometer (Optronics International, System P1000) and the linear coordinates for each diffraction spot recorded. These coordinates were then entered into the *CCP*4 *LAUE* package (Campbell *et al.*, 1987; Helliwell *et al.*, 1989) and the diffraction pattern indexed.

In order to improve the spatial resolution, and hence improve defect visualization, monochromatic X-rays from a monolithic (channel-cut) (111) silicon crystal with two symmetric reflections was employed. The divergence of the synchrotron radiation beam incident on the monochromator was $6 \times 60\,\mu\text{rad}^2$ (3×30 cm). The wavelength was chosen to be 1 Å, a wavelength frequently used in structure determination data collection. The crystal-to-film distance in this case was 75 mm and exposures took several minutes. The resulting images resolve features down to about 1 μm with separations of a few μm. Visually the images resemble electron micrographs, although, since there is no magnification the length scales represented are quite different.

Two weeks after the topographic studies some of the crystals were taken to beamline X12B of the NSLS for diffraction data collection. This beamline is equipped with a MAR Research imaging-plate detector, an Si (111) monochromator and a set of focusing mirrors.

The same wavelength used in the topographic studies was chosen for the monochromatic diffraction data collection, 1.0 Å. The sample-to-detector distance was about 190 mm, the rotation angle 1° and the exposure time 90 s. Because of beamtime constraints it was not possible to collect a full data set from all the crystals; a full data set was collected only for sample 26-3. The diffraction patterns were indexed and integrated with the *HKL* package (Otwinowski, 1993*a*,*b*; Minor, 1993).

4. Results

4.1. *X-ray topography*

The as-grown crystal and the enlarged (1 −1 0) white-beam X-ray topograph of sample 14 are shown in Fig. 1. The direction of the incident X-ray beam was a few degrees off the ⟨011⟩ crystallographic direction. The edges of the crystal in the topograph (Fig. 1*b*) are diffuse and two kinds of lines can be observed in the image. The first kind, *D* in the figure, is presumably an array of dislocations that originated at internal defects such as inclusions or grain boundaries which are usually surrounded by high stresses. Nucleation around such defects (inclusions or grain boundaries) often leads to dislocation bundles radiating from the seed. The second kind, *S* in the figure, is badly resolved, but one can see an array of lines parallel to the ⟨001⟩ crystallographic direction. Identification is impossible because of the low geometrical resolution of the image, a consequence of the large sample-to-film distance (300 mm).

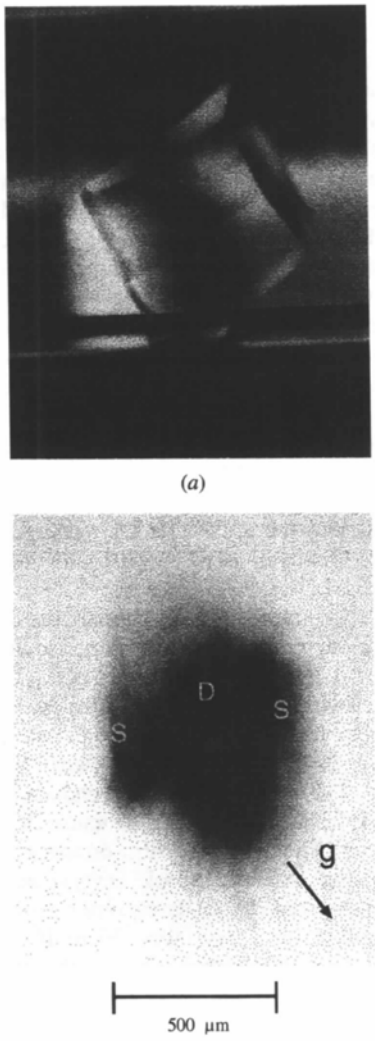

(*a*)

(*b*)

Fig. 1. (*a*) As-grown HEW lysozyme crystal, sample 14. (*b*) (1 −1 0) white-beam diffraction topograph; *D*, most probably an array of dislocations originated at grain boundaries or internal defects such as inclusions, and *B* linear defects parallel to the ⟨011⟩ crystallographic direction. Sample-to-film distance, 300 mm.

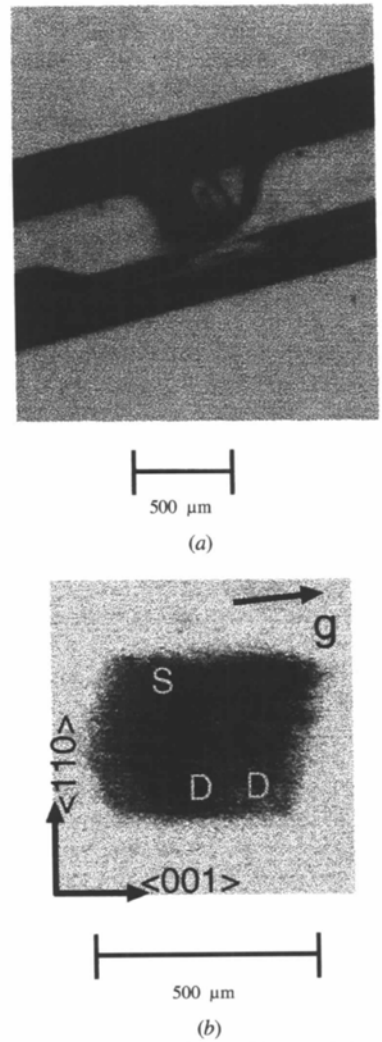

(*a*)

(*b*)

Fig. 2. (*a*) Crystal 25-1, grown from a Sigma solution (see Table 1), before exposure to the X-ray beam. (*b*) Monochromatic diffraction topograph; *S*, growth striations parallel to the ⟨001⟩ crystallographic direction, *D*, dislocation arrays in the ⟨011⟩ crystallographic direction. Sample-to-film distance 75 mm, wavelength 1.0 Å, resolution shell 2.3 Å.

In Fig. 2 the crystal, before exposure to the X-ray beam, and a monochromatic topograph are shown for sample 25-1. Two different kinds of defect can be observed in the topograph (Fig. 2*b*); two features in the ⟨110⟩, *D* in the figure, and several lines parallel to the ⟨001⟩, *S* in the figure. The two features, *D*, are not well resolved, but resemble dislocation arrays seen in other materials. These lines seem to be correlated with optically visible features in the crystal (Fig. 2*a*). The dark lines parallel to the ⟨001⟩ are most likely the result of varying levels of impurity incorporation, commonly referred to as growth striation bands. Similar patterns, as observed in Fig. 2(*b*), were obtained for crystal 25-2, grown from the same Sigma solution (5% impurity content). The same pattern was observed with crystals grown by the dialysis method, from a different Sigma batch (Stojanoff, Siddons, Snell & Helliwell, 1996), but not in crystals grown by the hanging-drop method from previously purified Sigma solutions (Stojanoff & Siddons, 1996).

The crystals grown from the purer Seikagaku solutions showed quite different structural quality. In Fig. 3 the as-grown crystal and a monochromatic topograph are shown for sample 26-1. An inclusion in the crystal is likely to be associated with a higher content of precipitant and impurities in the initial growth region (Vekilov, Monaco, Thomas, Stojanoff & Rosenberger, 1996) and could be observed under a light microscope and can be seen in Fig. 3(*a*). The topograph in Fig. 3(*b*), shows a highly strained central region, and two kinds of

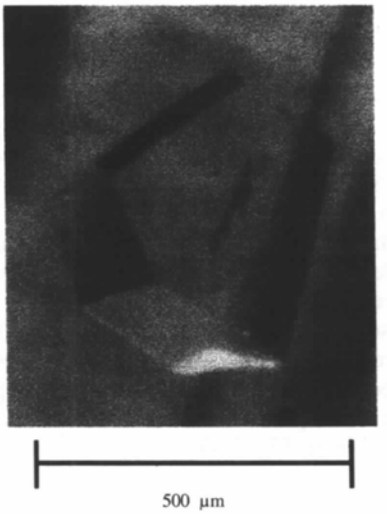

(*a*)

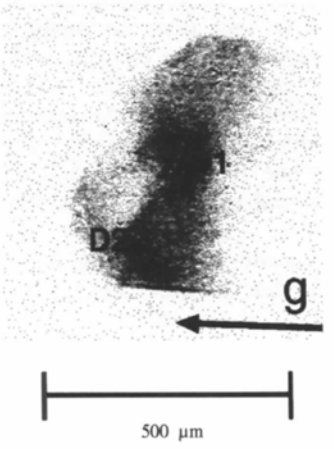

(*b*)

Fig. 3. (*a*) Crystal 26-1, as-grown tetragonal HEW lysozyme grown from a Seikagaku solution; for details see Table 1. (*b*) Monochromatic diffraction topograph; the line of no contrast observed in the central region is probably due to a precipitate, *D*1 and *D*2 are presumably dislocation arrays, for further discussion see text. Sample-to-film distance 75 mm, wavelength 1.0 Å, resolution shell 2.8 Å.

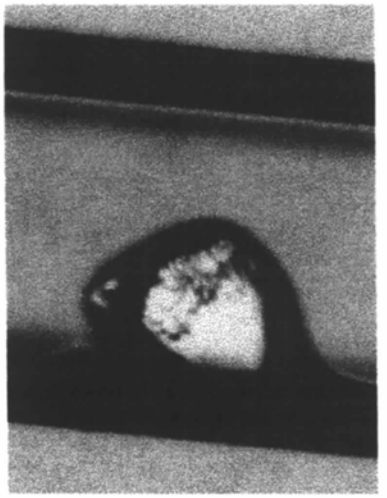

(*a*)

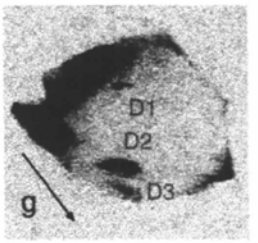

(*b*)

Fig. 4. (*a*) Crystal 26-3, tetragonal HEW lysozyme grown from a Seikagaku solution (Table 1), before exposure to X-rays. (*b*) Monochromatic diffraction topograph; *D*1, *D*2 and *D*3 are presumably small inclusions or dislocations; the dark regions around the border of the crystal are probably due to mechanical damage, a few linear defects can be observed in these regions. Sample-to-film distance 75 mm, wavelength 1.0 Å, resolution shell 3.1 Å.

features, $D1$ and $D2$ in the figure. The lack of contrast in the central region is typical of a precipitate; a line of no contrast (NC) perpendicular to the diffraction vector **g** is usually observed (Tanner, 1976).

The few short lines ($D1$) parallel to $\langle 001 \rangle$ in Fig. 3(b) are probably dislocations formed to relieve the strain around the precipitate. The feature, $D2$ in Fig. 3(b), seems to have been caused by mechanical damage to the crystal during the drainage of the capillary, just prior to the X-ray exposure. Fig. 4(a) shows sample 26-3 mounted in the X-ray capillary and Fig. 4(b) a monochromatic topograph of the same sample. A large perfect region and a highly strained border region can be observed in the topograph. Only a few features, $D1$, $D2$ and $D3$ are present in the larger otherwise perfect region. The linear defects observed in these features could be caused by small inclusions or dislocations. Linear defects in a highly strained region can be observed around the border of the crystal. As before, these defects were probably caused by mechanical damage to the crystal.

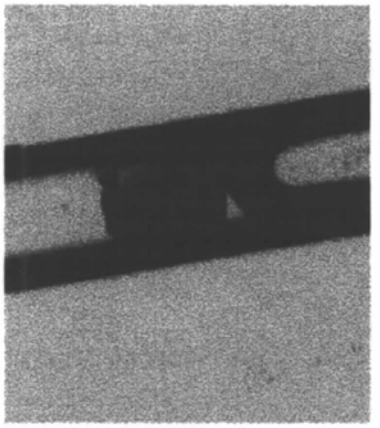

(a)

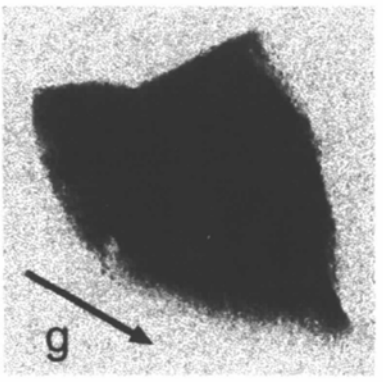

(b)

Fig. 5. (a) Crystal 28 after exposure to the X-ray beam, see Table 1 for growth conditions. (b) Monochromatic X-ray topograph, the high strain does not allow any speculation about the nature of defects. Sample-to-film distance 75 mm, wavelength 1.0 Å, resolution shell 3.7 Å.

Table 2. *Summary of results from monochromatic diffraction data collection for some of the samples submitted to monochromatic X-ray topography*

The data were integrated and scaled with the *HKL* suite (Otwinowski, 1993*a*,*b*).

Samples	25-1	26-1		26-3	
Total oscillation (°)	42	42	42	42	89
Overall crystal reflecting range (°)	0.299	0.080	0.083	0.074	0.080
Resolution limit (Å)	2.0	2.0	1.7	2.0	1.65
Completeness (%)	82.0	84.3	87.5	95.8	99.1
R scale (%)	5.7	3.4	3.7	3.6	5.3

The effect of temperature instabilities on the perfection of a crystal is shown in the topograph in Fig. 5. The topograph, from sample 28 also grown from the purer Seikagaku solution, but submitted to several changes in temperature during growth (see Table 1), is representative of a high strain level. With such a large level of defects it is impossible even to speculate on their nature. The observed strain is probably related to the veils (solvent inclusions, dislocations, *etc.*) that were shown to result from such temperature changes (Monaco & Rosenberger, 1993) which are always present in crystallization experiments under ambient conditions, and are visible in Fig 5(a).

4.2. *Diffraction*

A section of the diffraction patterns of some of the crystals after X-ray diffraction topography is shown in Fig. 6. As can be seen from the figure the diffraction spots from sample 25-1 are elongated overlapping and diffuse, while those for crystals 26-1 and 26-3 are round well separated and sharp. For the sake of comparison a section of the diffraction pattern of sample 28 is also shown in the figure (Fig. 6b). The results from the integration and scaling of the individual sets are presented in Table 2 and Fig. 7. The cut-off resolution limit was chosen after observation of the signal-to-noise ratio, $I/\sigma(I)$, for the different resolution shells. A plot of the percentage of reflections with $I/\sigma(I) > 20$ as a function of resolution is shown in Fig. 7(a) for samples 25-1 (dashed line) and 26-3 (solid line). As can be seen in this figure the percentage of reflections with $I/\sigma(I) > 20$ is very small for crystal 25-1 for resolutions lower then 2.0 Å. Therefore, in Table 2 in addition to the results shown for the available data on each of the samples, the results for 42° of data integrated and scaled only up to the 2.0 Å resolution shell are also shown for samples 26-1 and 26-3. For both samples 25-1 and 26-3 a comparison by resolution shell between the completeness and R scale is shown in Figs. 7(b) and 7(c).

The R factor is of the order of 35% larger for sample 25-1, while the $I/\sigma(I)$ is about a factor of two smaller compared with sample 26-3.

5. Discussion

Several authors (Durbin & Feher, 1900; Vekilov, Ataka & Katsura, 1993; Vekilov & Rosenberger, 1996) have attributed the growth process of tetragonal HEW lysozyme to dislocation-led growth and to two-dimensional nucleation processes depending on the supersaturation level. For intermediate supersaturations, similar to the present growth conditions, both mechanisms seem to coexist, growth islands and dislocations were observed. Recently, Nadaraja, Forsythe & Pusey (1995) have argued that the growth process cannot only be explained by dislocation-led growth or two-dimensional nucleation but should also take into account the incorporation of higher order lysozyme aggregates present in the growth solution (Boué, Lefaucheux, Robert & Rosenman, 1993). These

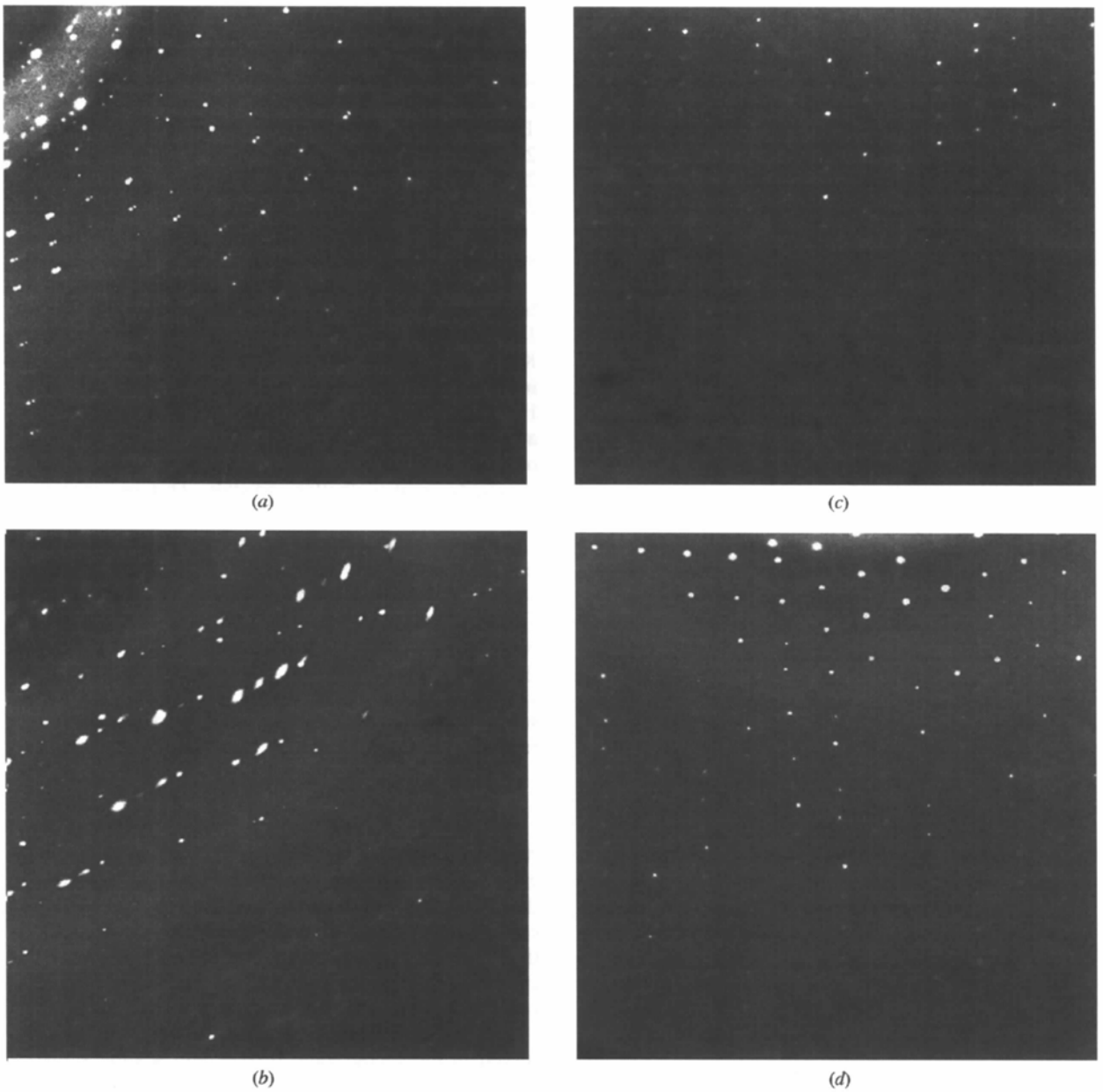

Fig. 6. Sections of diffraction patterns from crystals (*a*) 25-1 (resolution seen: 2.0 Å), (*b*) 28 (resolution seen: 2.5 Å), (*c*) 26-1 (resolution seen: 1.5 Å) (c) and (*d*) 26-3 (resolution seen: 1.5 Å). See text for exposure times and crystal-to-film distance.

aggregates may act as impurities and be incorporated in the crystal or act as growth units. These mechanisms may explain the growth striations observed in the ⟨110⟩ plane (Fig. 2*b*). as well as the anisotropic precipitate and linear defects observed in Fig. 3.

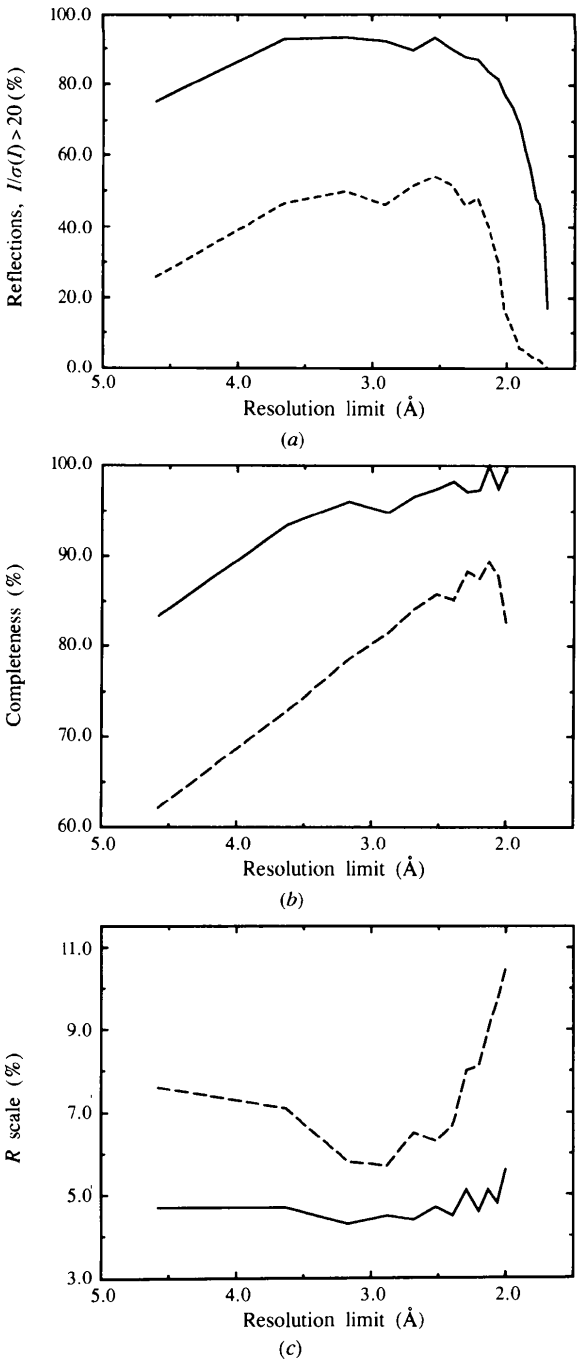

Fig. 7. Diffraction statistics for crystals 25-1 (dashed line) and 26-3 (solid line) *versus* resolution limit. (*a*) Fraction of reflections with signal-to-noise ratio $I/\sigma(I) > 20$; (*b*) completeness; (*c*) *R* scale factor. The statistics corresponds to that obtained with the *HKL* package (Otwinowski, 1993*a*,*b*)

The quality of a protein crystal is usually accessed through its mosaicity and diffraction resolution limit obtained from the analysis of diffraction patterns with programs such as the *HKL* package (Otwinowski, 1993*a*,*b*; Minor, 1993). These programs do not give true mosaicity values, but only an average value which is convoluted with an experimental function characteristic of the specific experimental setup used (crystal size, detector resolution, *etc.*). Nevertheless it was possible to observe a relationship between the X-ray topographs shown in Figs. 2, 3, 4 and 5 and the values listed in Table 2. Crystals which presented a higher density of defects presented overall worse diffraction properties. Sample 25-1b which shows a high concentration of striations in the topograph presents the highest mosaicity as well as the poorest diffraction resolution limit. A lower average signal-to-noise value was also observed for this sample. The statistical results from the oscillation data of crystals 26-1 and 26-3 are very similar; the mosaicity of sample 26-1 is about 7.5% higher then the mosaicity of sample 26-3. This result is in agreement with the topographic images of the two samples; crystal 26-3 presents a smaller density of defects.

Recently, detailed evaluations of crystal quality have been performed by several authors (Helliwell, 1988, 1992; Colapietro *et al.*, 1992; Fourme, Ducruix, Riès-Kautt & Cappelle, 1995). The mosaicity reported for individual reflections from microgravity and earth-grown HEWL crystals was of the order of a few hundredths of a degree for the best crystals (Snell, *et al.*, 1995). All of the above authors make the assumption that lower mosaicity implies 'better' crystals. This assumption is also supported by the present results.

The diffraction resolution limit shown in Table 2 is also a result from the *HKL* package (Otwinowski, 1993*b*). Although there is measurable diffraction up to 1.55 Å and probably beyond, for sample 26-3, the signal-to-noise ratio was really too small to allow reflections lying in higher resolution shells to be taken into account by the scaling procedure. Both the experimental setup and beamtime limitations did not allow for higher resolution data collection on that sample.

6. Summary and conclusions

X-ray topographic methods were used to characterize growth defects in hen egg-white lysozyme crystals. To the extent that high-resolution diffraction-data collection could be performed after X-ray diffraction topography this method proved to be non-destructive to protein crystals. Furthermore it showed the dependence of defect concentration as a function of growth conditions.

The good correlation between the defect density observed in the topographic images and scaling statistics shows that X-ray topography can be used to access crystal quality if not in a quantitative way at least from a qualitative point of view. Probably, its best application

will be, in combination with rocking-curve measurements, as a survey tool to improve macromolecular crystal growth techniques but it could also help to understand problems such as changes in mosaicity arising from freezing, degradation on soaking of derivatives, *etc.*

The authors would like to thank Ms G. Shea and the BioCars group for their technical support at the X26C beamline at the NSLS/BNL. They are also indebted to Mr D. Berman, Mr N. Tempel and Ms H. Kycia. This work was supported by NSF (Grant No. DMB-9104630), NASA (Grant No. NAG8-950) and the State of Alabama through the Center for Microgravity and Materials Research at the University of Alabama in Huntsville, USA. NSLS is funded by the US Department of Energy under contract number DE-AC02-76CH00016.

References

Campbell, J. W., Clifton, I. J., Elder, M., Machin, P. A., Zurek, S., Helliwell, J. R., Habash, J., Hajdu, J. & Harding, M. M. (1987). *Biophysics and Synchrotron Radiation, Springer Series in Biophysics,* Vol. 2, edited by A. Bianconi & A. Congiu Castellano, pp. 52–60. Berlin: Springer-Verlag.

Colapietro, M., Cappucio, G. Marciante, C., Pifferi, A., Spagna, R. & Helliwell, J. R. (1992). *J. Appl. Cryst.* **25**, 192–194.

Durbin, S. D. & Feher, G. (1900). *J. Mol. Biol.* **212**, 763–774.

Fourme, R., Ducruix, A., Riès-Kautt, M. & Capelle, B. (1995). *J. Synchrotron Rad.* **2**, 136–142.

Helliwell, J. R. (1988). *J. Cryst. Growth*, **90**, 259–272.

Helliwell, J. R. (1992). *Macromolecular Crystallography with Synchrotron Radiation*, ch. 2. pp. 24–26. Cambridge University Press.

Helliwell, J. R., Habash, J., Cruickshank, D. W. J., Harding, M. M., Greenhough, T. J., Campbell, J. W., Clifton, I. J., Elder, M., Machin, P. A., Papiz, M. Z. & Zurek, S. (1989). *J. Appl. Cryst.* **22**, 483–497.

Minor, W. (1993). *XDisplayF*. Purdue University, West Lafayette, Indiana, USA.

Monaco, L. A. & Rosenberger, F. (1993). *J. Cryst. Growth*, **129**, 465–484.

Otwinowski, Z. (1993*a*). *Oscillation Data Reduction Program, Proceedings of the CCP4 Study Weekend*, edited L. Sawyer, N. Issacs & S. Bailey, pp. 56–62. Warrington: Daresbury Laboratory.

Otwinowski, Z. (1993*b*). *SCALEPACK*. Yale University, New Haven, Connecticut, USA.

Rosenberger, F., Howard, S. B., Sowers, J. W. & Nyce, T. A. (1993). *J. Cryst. Growth*, **129**, 1–12.

Rosenberger, F., Muschol, M., Thomas, B. R. & Vekilov, P. G. (1996). *J. Cryst. Growth*, **168**, 1–27.

Snell E. H., Weisgerber, S., Helliwell J. R., E. Weckert, E., Holzer, K. & Schroer, K. (1995). *Acta Cryst.* D**51**, 1099–1102.

Stojanoff, V. & Siddons, D. P. (1996). *Acta Cryst.* A**52**, 498–499

Stojanoff, V., Siddons, D. P., Snell, E. H. & Helliwell, J. R. (1996). *Synchrotron Radiat. News*, **9**, 25–26.

Thomas B. R., Vekilov, P. G. & Rosenberger, F. (1996). *Acta Cryst.* D**52**, 776–784.

Vekilov, P. G., Ataka, M. & Katsura, T. (1993). *J. Cryst. growth*, **130**, 317–320.

Vekilov, P. G., Monaco, L. A. & Rosenberger, F. (1995). *J. Cryst. Growth*, **156**, 267–278.

Vekilov, P. G., Monaco, L. A., Thomas, B. R., Stojanoff, V. & Rosenberger, F. (1996). *Acta Cryst.* D**52**, 785–798.

Vekilov, P. G. & Rosenberger, F. (1996). *J. Cryst. Growth*, **158**, 540–551.

Tanner, B. K. (1976). *X-ray Diffraction Topography*, 1st ed. Oxford: Pergamon Press.